Phasor Measurement Unit based Fault Detection using Tellegen's Theorem in Geographically Zoned Power Systems

Mohammad Anas
Department of Electrical Engineering, Jamia Millia Islamia University

Sunil Kumar
Department of Electrical Engineering, Jamia Millia Islamia University

Md. Fazle Rasool
Department of Electrical Engineering, Jamia Millia Islamia University

Ikbal Ali
Department of Electrical Engineering, Jamia Millia Islamia University

https://doi.org/10.5109/7363494

出版情報：Evergreen. 12 (2), pp.1051-1062, 2025-06. Interdisciplinary Graduate School of Engineering Sciences, Kyushu University, Japan
バージョン：

Phasor Measurement Unit Based Fault Detection Using Tellegen's Theorem in Geographically Zoned Power Systems

Mohammad Anas[1], Sunil Kumar[1,*], Md. Fazle Rasool[1], Ikbal Ali[1]

[1]Department of Electrical Engineering, Jamia Millia Islamia University, New Delhi 110025, India

*Author to whom correspondence should be addressed:
E-mail: skk7503@gmail.com

(Received November 28, 2024; Revised March 07, 2025; Accepted April 24, 2025)

Abstract: To ensure system stability and minimize downtime, it is imperative to rapidly and precisely identify faults in power systems. This study proposes a method that utilizes Phasor Measurement Units (PMUs) and Tellegen's theorem for fault detection. The power system is divided into zones based on geographical and electrical attributes, with PMUs strategically positioned in each zone to monitor voltage and current phasors. By applying Tellegen's theorem to the collected data, faults within these zones can be pinpointed. Experimental results on an 8-bus power system demonstrate the effectiveness of this approach, showing both accurate fault identification and reduced computational complexity. The simulation modeling of IEEE 8 bus system is performed on the platform real time digital simulator (RTDS/RSCAD).

Keywords: fault detection; open circuit and closed-circuit faults; synchrophasor unit; RTDS; Tellegen’s theorem

1. Introduction

1.1. Motivation

The power system which consist a network of distribution generations (DGs), transmission lines (TL), transformers, and loads[1,2]. Despite the significant advances in power system technology, faults and disturbances still occur, causing interruptions in the power supply and potentially damaging equipment. Therefore, timely and accurate fault detection and identification are crucial for the safe and reliable operation of the power system. Model-based and data-driven methods make up the majority of the fault identification methods described in technical literature. Model-based fault identification methods simulate the behavior of the power system under fault situations utilizing mathematical models of the system[3–5]. By comparing the simulated and observed waveforms, these models may be used to anticipate the location and type of the fault. The ability to replicate the behavior of the power system under a variety of operating situations, including various fault kinds and varied loads, is one benefit of model-based fault identification methods. The precision of the mathematical models used to mimic the behavior of the power system, however, places constraints on model-based techniques. Data-driven fault identification techniques analyze the data from sensors to identify the faults through a approaches of Artificial Inteligence (AI) and Machine Learning[6,7]. To increase their accuracy and speed of fault detection and diagnosis, these systems can learn from past data. Data-driven approaches offer the benefit of being able to identify and categorize faults[8] that may not have been previously noticed or that have not been adequately described in the literature. This is due to the ability of machine learning (ML) algorithms to find patterns and correlations in the data that may be challenging for human professionals to recognize. Data-driven approaches do have a drawback in that they are ineffective without a substantial amount of high-quality training data. Regarding phasor measurement unit (PMU)-based fault detection, at various points across the power system PMUs can measured the phasor quantity of voltage and current at both end of buses[9,10]. As a result, faults may be found and identified quickly and accurately. Researchers have recently looked at the application of Tellegen's theorem and PMUs for fault detection in power systems[11,12].

1.2. Research gap

In the past ten years, numerous protection plans for microgrids designed by researchers have resulted in numerous complexities during their construction. In-depth examinations of the protection issues faced by microgrids, as highlighted by[13] over both AC and DC components. The implementation of Phasor Measurement Units (PMUs) has significantly improved fault detection in power systems by providing accurate, time-synchronized data, thereby enabling real-time monitoring and swift fault identification[14]. The study highlighted[15] the reliable

Cite: S. Kumar et al., "Phasor Measurement Unit based Fault Detection using Tellegen's Theorem in Geographically Zoned Power Systems". Evergreen, 12 (02) 1051-1062 (2025). https://doi.org/10.5109/7363494.

Table 1: Summary of literature review

Research Paper Title	Technique Used	Advantages	Disadvantages
"Fault Detection and Classification in Power Systems Using Wavelet Transform and Support Vector Machine" by [16]	Wavelet Transform and support vector machine	Accurate fault identification and classification	Appropriate wavelet parameter selection is necessary
"Expert System Based Fault Detection of Power Transformer " by [17]	Expert System	Provides a tool for making decisions to detect and diagnose faults.	Expert expertise is needed to create the system.
"Fault Diagnosis of Machines Based on D-S Evidence Theory. Part 1: D-S Evidence Theory and Its Improvement" by [18]	D-S evidence theory and decision tree algorithm	Effective fault classification and detection	Limitations of evidence theory's veracity
"Power System Fault Detection and Classification Using Improved Artificial Bee Colony Algorithm" by [19]	Artificial Bee Colony Algorithm	High accuracy in classifying and detecting faults	Demanding in terms of computation for large power installations
"A Deep Convolution Neural Network Based Fault Detection and Diagnosis for Power Transformers" by [20]	Deep convolution neural network	Highly effective in fault identification and diagnosis	Large amounts of data is needed to train the neural network
"Fault Classification in Power Systems Using Ensemble Empirical Mode Decomposition and SVM Classifier" by [21]	Ensemble empirical mode decomposition and support vector machine	Accurately detects and identifies faults	Proper selection of SVM parameters is required
"Hybrid modified evolutionary particle swarm optimization-time varying acceleration coefficient-artificial neural network for power transformer fault diagnosis" by [22]	Artificial neural networks and particle swarm optimization	Detect Faults with high precision and accuracy	Limited amount of training data is one of the major drawback

application of Tellegen's theorem in electrical network analysis to identify inconsistencies in power flow, providing a dependable mathematical framework for fault diagnosis. Research has shown that identifying system irregularities is effective by comparing predicted and actual power allocations [23]. The majority of current research has centered on small-scale or localized networks, and has conducted only a limited examination of geographically dispersed power systems. Accuracy in detecting faults in large-scale networks is impaired by problems such as communication delays, lost data, and environmental changes, as observed by [24]. Advanced machine learning and adaptive filtering techniques have led to improved classification accuracy, but more research is still needed to establish reliable, real-time fault detection methods that can efficiently handle these complex issues [25]. Table 1, gives a brief summary of literature review for various fault identification techniques.

1.3. Contribution

The main focus of the approach is to daignosis faults in the system by measureing the phasor quantity of voltage and current through PMU to calvulate active and reactive power. These powers are then compared to active and reactive power thresholds to determine open circuit (OC) & short circuit (SC) faults. Section-2 illustrate methodology used for fault detection and Section-3 describe the simulation result. Section-4 discussed final conclusion and last section represent the references.

2. Methodology

2.1. Proposed Methodology

A proposed methodology for identifying faults combines data from Phasor Measurement Units (PMUs) with analytical methods to identify and pinpoint faults in power systems segmented into specific geographic zones. The essential steps in this process are:

a) The initial step involves collecting coordinated data from a multitude of PMUs placed throughout the power system [26,27]. Key components of power systems, including transmission lines, transformers, and generators, should be strategically positioned throughout the system.

b) In second step, the active and reactive powers transmitted through the cross-section of a power system can be calculated using data from a PMU [28]. The active power can be calculated using the real parts of voltage and current phasors, while the reactive power can be determined from the imaginary parts of these phasors.

c) In third step, the thresholds for open-circuit and short-circuit faults can be determined based on the anticipated total power. The power system's integrity is compromised when the cumulative amount of power crossing its cross section exceeds a predetermined threshold [29].

d) The next step involves the identification of open-circuit or short-circuit faults is facilitated through the use of

symmetrical components of voltages and currents [30]. The sequences of voltages (V_{a0}, V_{a1}, V_{a2}) & currents (I_{a0}, I_{a1}, I_{a2}) are computed from the respective voltages (V_a, V_b, V_c) and currents (I_a, I_b, I_c).

e) In last step, the fault location is calculated using the voltage and current variances at each bus, combined with the faulted line impedance [31]. The location of the fault was determined to be the distance between the PMU and the fault.

2.2. Selection Criteria for Zone Division and PMU Placement

This section outlines the criteria employed in this research for dividing the 8-bus test power system into zones and determining PMU placement by follow the essential steps: The first step involves obtaining the one-line diagram of the eight-bus test power system. The second step identify the key lines and buses that are critical to the functioning of the system. To identify the lines with the greatest power flows, a power flow analysis must be conducted, a procedure critical for maintaining both system stability and reliability.

The third step determine the maximum separation between the PMUs based on the measurement resolution and transmission capacity. PMUs can be placed within an acceptable distance of 80-100 km. The system is divided into zones according to critical lines and buses in step four. Each zone contains a group of key power lines and buses located in close proximity to one another and within a predetermined maximum distance between the PMUs.

The last Step involves installing PMUs at the boundaries of each zone to record the voltage and current phasor values at both the pre-fault and post-fault stages of the designated zones.

2.3. Setting Fault Detection Thresholds

When setting fault detection thresholds, we must define the expected range of active and reactive powers under typical operating conditions and establish limits for acceptable departures from this range during faults when setting fault detection thresholds [32]. The characteristics of the power system, such as the voltage level, system impedance, and load demand, determine the exact ranges of the thresholds. Using statistical methods such as the standard deviation of the active and reactive powers; we have determined the expected ranges of power during normal operation. Using these ranges, we set the thresholds for open-circuit and short-circuit faults as follows:

2.3.1. Data Collection

During normal operation, historical information about the active and reactive powers of the power system is gathered. This information should be accurate and depict the changes in the load conditions over a representative period.

2.3.2. Calculating mean and standard deviation

Using the pre-processed data, the mean values of the active and reactive powers and standard deviation are determined. The standard deviation measures the variability or dispersion of the power levels around the mean, whereas the mean reflects the average power level.

Active Power Mean ($\bar{P}$) = $\frac{\sum_0^N P_i}{N}$

Reactive Power Mean ($\bar{Q}$) = $\frac{\sum_0^N Q_i}{N}$

Active Power Standard Deviation (σ_p) = $\sqrt{\frac{\Sigma(P-P')^2}{N-1}}$

Reactive Power Standard Deviation (σ_q) = $\sqrt{\frac{\Sigma(Q-Q')^2}{N-1}}$

2.3.3. Determine Confidence Level Thresholds

The confidence level based on the desired accuracy level is selected. Using the mean and standard deviation, the upper and lower limits for the active and reactive powers were established. The symbols mean plus and mean minus of the standard deviation are used to calculate the upper and lower threshold values, respectively. The specific multiple is defined by the chosen confidence level as follows:

Active Power Upper Threshold = $\overline{\mathrm{P}} + \mathrm{m} \times \sigma_p$

Active Power Lower Threshold = $\overline{\mathrm{P}} - \mathrm{m} \times \sigma_q$

Reactive Power Upper Threshold = $\overline{\mathrm{Q}} + \mathrm{m} \times \sigma_q$

Reactive Power Lower Threshold = $\overline{\mathrm{Q}} - \mathrm{m} \times \sigma_q$

where ‘m’ is the multiple based on the confidence level.

2.3.4. Fault Detection

Monitoring the active and reactive powers continuously throughout real-time operation will identify faults. The presence of a defect is indicated by a power level that deviates from the predicted range and defined thresholds.

2.4. Open circuit fault

In an open circuit fault, the current path is interrupted, and no current can flow through the faulted bus. The active power is the product of the voltage and current. The absence of current through the bus reduced the active power. In an open-circuit fault condition, the absence of current flow through the faulted bus can cause voltage rise. This increase in voltage can lead to a decrease in reactive power [33,34]. Hence, if the active power goes below the lower threshold limit (P_L) and the reactive power also goes beyond the lower threshold limit (Q_L), short circuit fault will be detected.

2.5. Short circuit fault

When an SC fault occurred, a heavy current started to flow suddenly in the conductor through the faulted bus and with the associated components of the faulted buses. The fault current is caused by voltage fall among the faulted buses, which decreases the active power at that bus [35,36]. Therefore, the reactive power on the bus tends to increase.

Cite: S. Kumar et al., "Phasor Measurement Unit based Fault Detection using Tellegen's Theorem in Geographically Zoned Power Systems". Evergreen, 12 (02) 1051-1062 (2025). https://doi.org/10.5109/7363494.

Hence, if the active power goes below the lower threshold limit (P_L) and the reactive power goes above the upper threshold limit (Q_H), then a short-circuit fault is detected.

2.6. Fault Line Impedance & Fault Location Calculations

A single line diagram of two transmission lines is illustrated in Figure 1, where a fault occurs at point F. The PMU was installed at both ends of the buses, and it measured the phasor values of the sending and receiving voltages and the current of the transmission line. These phasor values are used to calculate the impedance and to identify the fault location. The per unit distance technique 37,38) was used to identify faults and measure the impedance of the transmission line in the ohms. The network is illustrated in Figure 1 comprises a homogeneous transmission line that connects terminals G and H. The transmission line has a total positive-sequence impedance of Z_{L1}. The equivalent circuit between terminals G and H is determined by their individual Thevenin's theorem, denoted as Z_G and Z_H respectively.

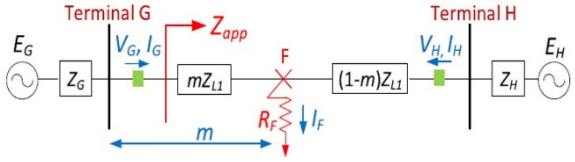

Fig. 1: One Line Diagram of Two Terminal Transmission Line

The proposed approaches use the voltage and current recorded at terminal G or terminal H, even though measured quantities are available at both ends of the transmission line. The voltage drop in the transmission line between terminal H and G, are determined by applying Kirchhoff's rules written in equation (1) as,

$$V_G = mZ_{L1}I_G + R_F I_F \qquad (1)$$

where voltage and current at terminal G is denoted as V_G and I_G respectively, which depend on the type of faults. The apparent impedance (Z_{app}) is calculated by solving the equation (1) expressed as,

$$Z_{app} = \frac{V_G}{I_G} = mZ_{L1} + R_F \left(\frac{I_F}{I_G}\right) \qquad (2)$$

Where fault resistance is denoted as R_F. However, measurements are only taken from one end of the line, equation (2) has three unknowns: m, R_F, and I_F.

2.7. Simple Reactance Method

The straightforward reactance technique exploits the resistive nature of the fault resistance R_F. As a result, the phrase $R_F \frac{I_F}{I_G}$ in equation (2) simplifies to a real number as seen in Figure 2, if currents I_F and I_G are considered to be in phase.

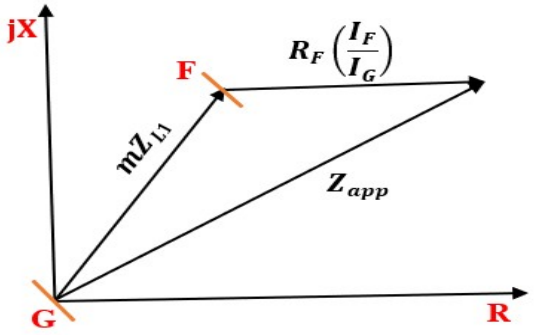

Fig. 2: Reactance Error in Simple Reactance Method

The distance to a fault can be calculated by resolving equation (2) into its imaginary parts.

$$m = \frac{img\left(\frac{V_G}{I_G}\right)}{img(Z_{L1})} \qquad (3)$$

The simple reactance method was used to calculate the reactance of the buses while ignoring the fault resistance at the identified fault location. The overall purposed methodology is illustrated through a flowchart in Figure 3.

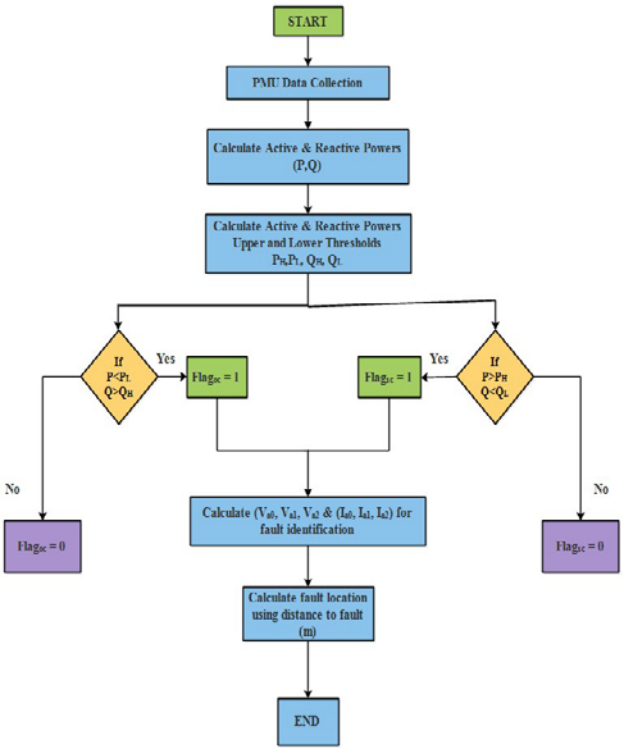

Fig. 3: Flowchart of proposed approach

A sample radial test system incorporating distributed generators is depicted in Figure 4, to demonstrate the terminology employed in this research work.

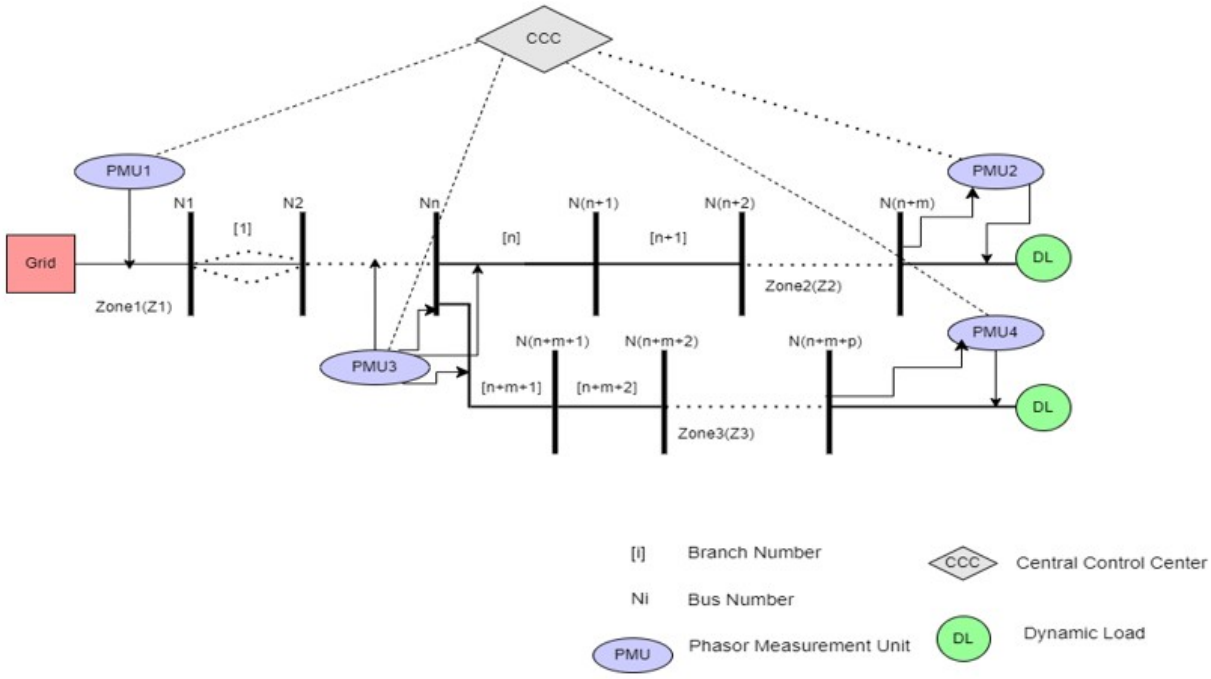

Fig. 4: Single Line Diagram of sample test case with CCC & DL

The sample network was divided into three distinct zones (Z_1, Z_2, and Z_3), comprising a total of (n + m + p) nodes. In this study, the 8 bus test power systems were partitioned into 4 distinct areas, with the key transmission lines, buses, and PMUs located at the outer edges of each area used to monitor the phasor voltage and current.

3. Result Discussion

The main elements comprising the 8-bus test power system comprised 230-kV AC source, fault inception logic, Bergeron-type transmission lines, dynamic load components, current transformers (C.T's), potential transformers (P.T's), and circuit breakers. Two parallel transmission lines, denoted as transmission lines 1 and 2, establish the connection between the source and the load within the test system.

The system is equipped with four circuit breakers namely BRK_1, BRK_2, BRK_3, and BRK_4. Breakers BRK_3 and BRK_4 are located along transmission line 1, whereas breakers BRK_1 and BRK_2 are positioned on transmission line 2. The current transformer operates with a CT ratio of 300:1, nominal RMS current of 646 A, and output RMS current of 2.15 A. The potential transformer maintains a nominal RMS voltage of 230 kV for the three phases and 132 kV for the output phase.

3.1. Power Thresholds Calculations

Power threshold calculations involve determining the critical power levels within a system to ensure its stability and reliability. These thresholds are crucial for identifying potential faults or abnormalities that could lead to system failures or downtime. Calculations typically consider factors such as maximum power flow limits, equipment ratings, and operational constraints. The calculated active and reactive power thresholds are presented in Table 2 and Table 3.

Table 2: Active Power Calculation

P	$(\mathbf{P}-\overline{\mathbf{P}})$	$(\mathbf{P}-\overline{\mathbf{P}})^{\mathbf{2}}$
6361	−434	188356
6562	−233	54289
7401	606	367236
7610	815	664225
6120	−675	455625
6001	−794	630436
7300	505	255025
7400	605	366025
6402	−393	154449

Mean of Active Power $(\bar{P}) = \frac{\sum P}{N} = 6795$

Standard Deviation of Active Power$(\mathfrak{6}_{\boldsymbol{p}}) = \sqrt{\frac{\sum(P-\bar{P})^2}{N-1}}$

$= 626.065$

Active Power Upper Threshold $(P_H) = \overline{\mathrm{P}} + \mathrm{n} \times \sigma_p$

Active Power Lower Threshold $(P_L) = \overline{\mathrm{P}} - \mathrm{n} \times \sigma_p$

In our case, we select the value of "n" as an integer determined by the confidence level, and we choose it to be 2. Consequently, the equations are then transformed as follows:

Active Power Upper Threshold $(P_H) = \overline{\mathrm{P}} + 2 \times \sigma_p$

$= 8047.13$ KW

Active Power Lower Threshold $(P_L) = \overline{\mathrm{P}} - 2 \times \sigma_p$

= 5542.847 KW
where P is measured in Kilowatts (KW).

Table 3: Reactive Power Calculation

P	$(P-\bar{P})$	$(P-\bar{P})^2$
6361	−434	188356
6562	−233	54289
7401	606	367236
7610	815	664225
6120	−675	455625
6001	−794	630436
7300	505	255025
7400	605	366025
6402	−393	154449

Mean of Reactive Power $(\bar{Q}) = \frac{\sum Q}{N} = 54.67$

Standard Deviation of Active Power$(\sigma_q)=\sqrt{\frac{\sum(Q-\bar{Q})^2}{N-1}}$
= 8.49

Reactive Power Upper Threshold $(Q_H) = \bar{Q} + 2 \times \sigma_q$
= 71.66 KVar

Reactive Power Lower Threshold $(Q_L) = \bar{Q} - 2 \times \sigma_q$
= 37.68 KVar

where Q is measured in kilovolt-amperes reactive (Kvar).

3.2. Identification of Short Circuit Faults

This phenomenon creates an irregular current flow that can cause overheating, equipment damage, and potentially dangerous situations. The waveforms of the voltage and current before the fault at bus 5 are illustrated in Figure 5 and Figure 6 respectively. The proposed fault detection approach 39) demonstrated for short circuit fault types.

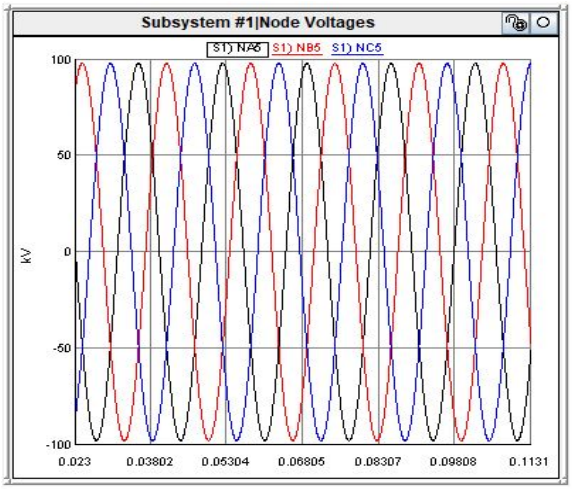

Fig. 5: Voltage at bus 5 before the fault

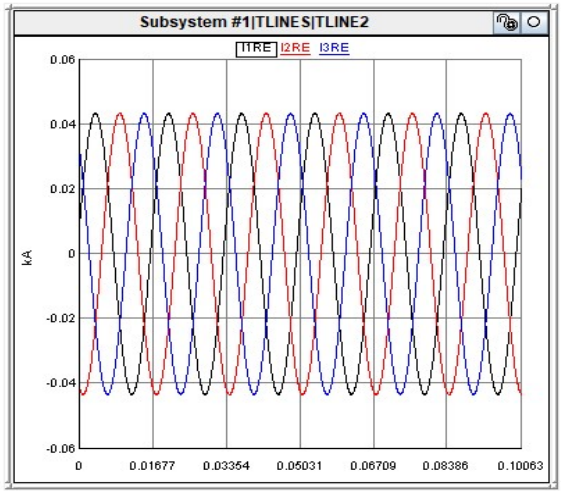

Fig. 6: Current at bus 5 before the fault

3.2.1. Line to Ground fault (LG)

In this case, an LG fault is simulated on bus 5. The voltage and current waveforms after the LG fault are shown in Figure 7 and Figure 8. The calculated active and reactive powers at bus 5 were 5308.491 kW and 136.7 KVar. The active power on bus 5 exceeded the upper threshold limit. Hence, a short circuit fault was detected at bus 5.

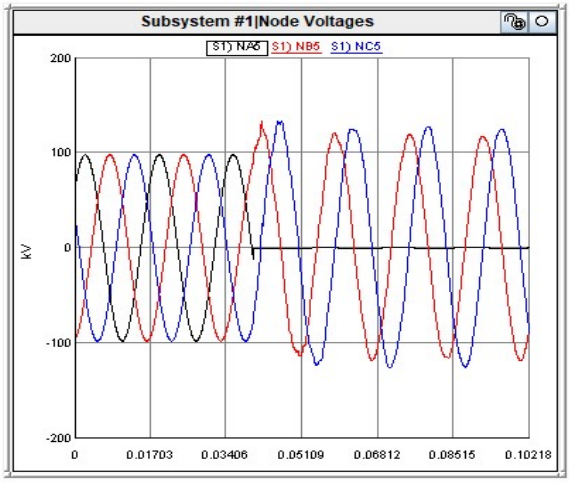

Fig. 7: Voltage waveform at bus 5 after LG fault

The three complex power, active and reactive power is calculated as,

3-ϕ Complex Power $(S_{3-\varphi}) = V_a I_a + V_b I_b + V_c I_c$

3-ϕ Active Power = Real $(S_{3-\varphi})$ = 5308.491 KW

3-ϕ Reactive Power = Img $(S_{3-\varphi})$ = 136.7 KVar

The symmetrical components of the current can be calculated to detect fault types.

$$I_{ao} = \frac{1}{3}(I_a + I_b + I_c) = 287.74\angle 2.568 \text{ A}$$

$$I_{a1} = \frac{1}{3}(I_a + \alpha I_b + \alpha^2 I_c) = 287.61\angle 2.436 \text{ A}$$

$$I_{a2} = \frac{1}{3}(I_a + \alpha^2 I_b + \alpha I_c) = 287.96\angle 2.489 \text{ A}$$

Cite: S. Kumar et al., "Phasor Measurement Unit based Fault Detection using Tellegen's Theorem in Geographically Zoned Power Systems". Evergreen, 12 (02) 1051-1062 (2025). https://doi.org/10.5109/7363494.

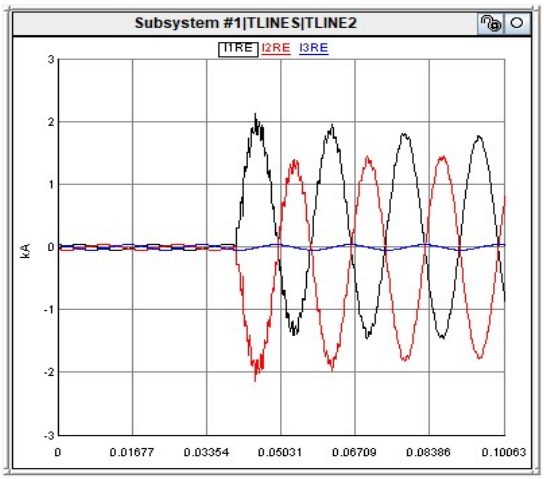

Fig. 8: Current at bus 5 after LG fault

It is evident that $I_{a0} = I_{a1} = I_{a2}$ are equivalent, which takes place during a single line to ground fault. The LG fault was subsequently pinpointed on bus 5. The LG fault location can be determined through equation 3, where m was found to be 68.43 km in the case of an LG fault from the source. The locations of different fault types can be found similarly.

3.2.2. Line to Line fault (LL)

In this case, an LL fault occurs at bus 5. The voltage decreases and current rises suddenly because of the shortcoming of the two phases, as depicted in Figure 9 and Figure 10, respectively. The pre-fault and post-fault magnitudes of the voltage and current were measured through the PMU, which further determined the three-phase active and reactive power.

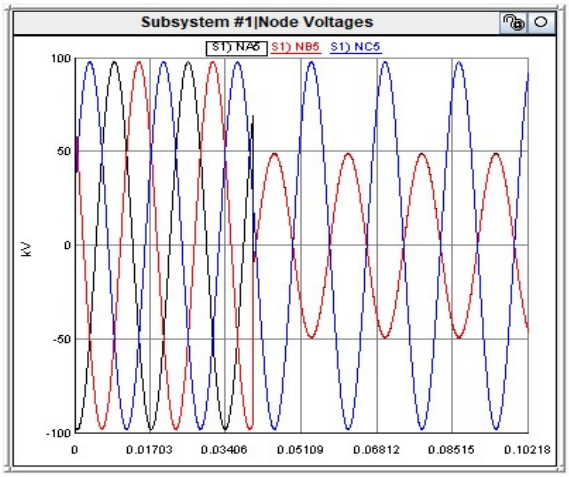

Fig. 9: Voltage at bus 5 after LL fault

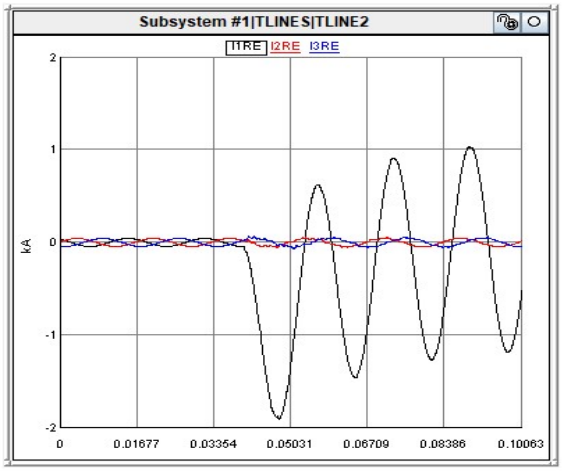

Fig. 10: Current waveform at bus 5 after LL fault

The active power exceeds the upper threshold limit; hence, a short circuit fault can be identified as follows:

3-ϕ Active Power = Real ($S_{3-\varphi}$) = 4573.29 KW

3-ϕ Reactive Power = Img ($S_{3-\varphi}$) = 102.56 KVar

$I_{ao} = \frac{1}{3}(I_a + I_b + I_c) = 0$

$I_{a1} = 351.45\angle 58.34$

$I_{a2} = -351.49\angle 58.65$

Since $I_{a1} = -I_{a2}$, an LL fault can be identified.

3.2.3. Line to Line Ground fault (LLG)

To simulate this scenario, an LLG fault was triggered at bus 5, and the active and reactive powers were calculated using the voltage and current phasor gathered from the PMUs. The voltage and current patterns following the LLG fault are shown in Figure 11 and Figure 12. Remarkably, the active power on bus 5 exceeds the upper threshold limit (P_H), which indicates the occurrence of a short circuit fault.

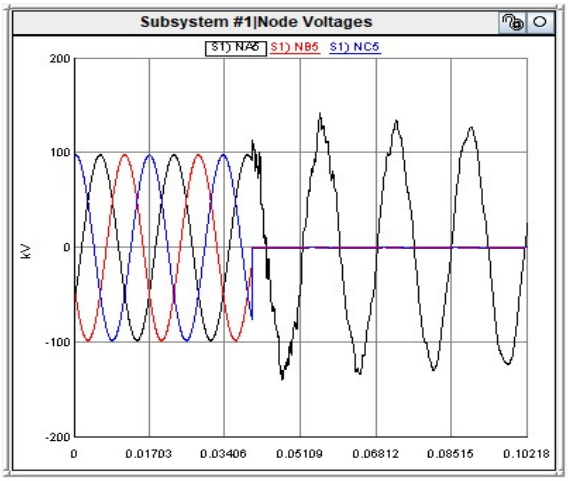

Fig. 11: Voltage waveform at bus 5 after LLG fault

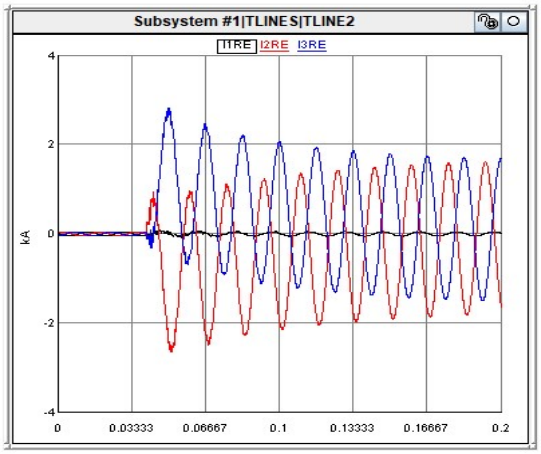

Fig. 12: Current waveform at bus 5 after LLG fault

To precisely identify the fault type, the symmetrical components of the voltages are computed.

3-ϕ Active Power = Real $(S_{3-\varphi})$ = 3373.708 KW

3-ϕ Reactive Power = Img $(S_{3-\varphi})$ = −86.695 Kvar

$$V_{a0} = \frac{1}{3}(V_a + V_b + V_c) = 29711.54\angle -2.0585$$

$$V_{a1} = \frac{1}{3}(V_a + \alpha V_b + \alpha^2 V_c) = 29592.19\angle -2.06$$

$$V_{a2} = \frac{1}{3}(V_a + \alpha^2 V_b + \alpha V_c) = 29591.98\angle -2.12$$

Since $V_{a1} = V_{a2}$, LLG fault is identified.

3.3. Identification of Open Circuit Faults

During an open circuit fault, one or more conductors may rupture, leading to an imbalance in current flow within the system 40). This type of fault can be classified as 1-conductor, 2-conductor, or 3-conductor open circuit faults. The voltage and current patterns prior to the open circuit fault at bus 5 are depicted in Figure 13. The phasors for voltage and current were extracted from the Phasor Measurement Unit (PMU) located at bus 5, and the calculations for active and reactive power at bus 5 were performed using these phasors.

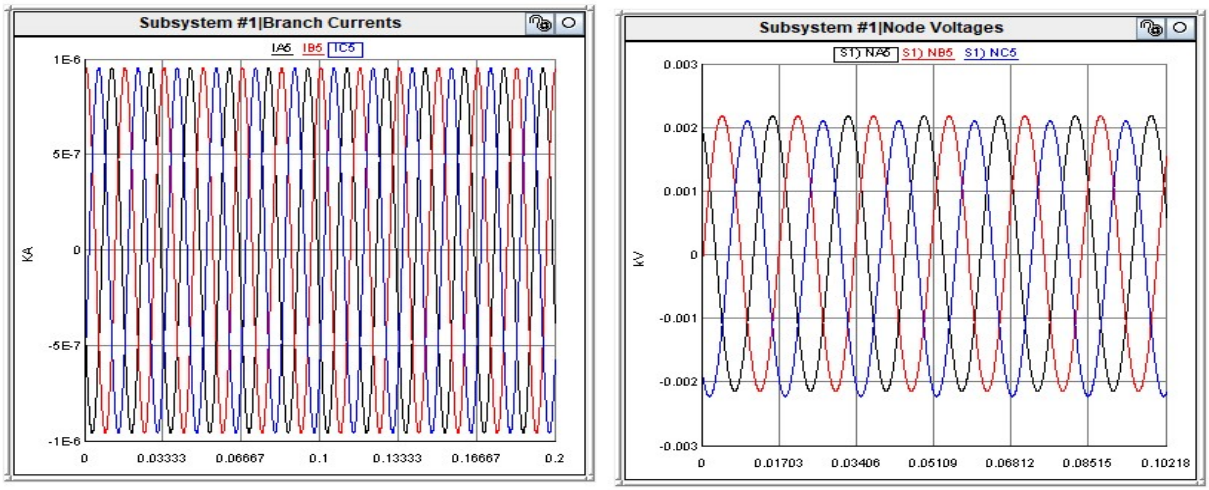

Fig. 13: Voltage and current waveforms at bus 5 before OC fault

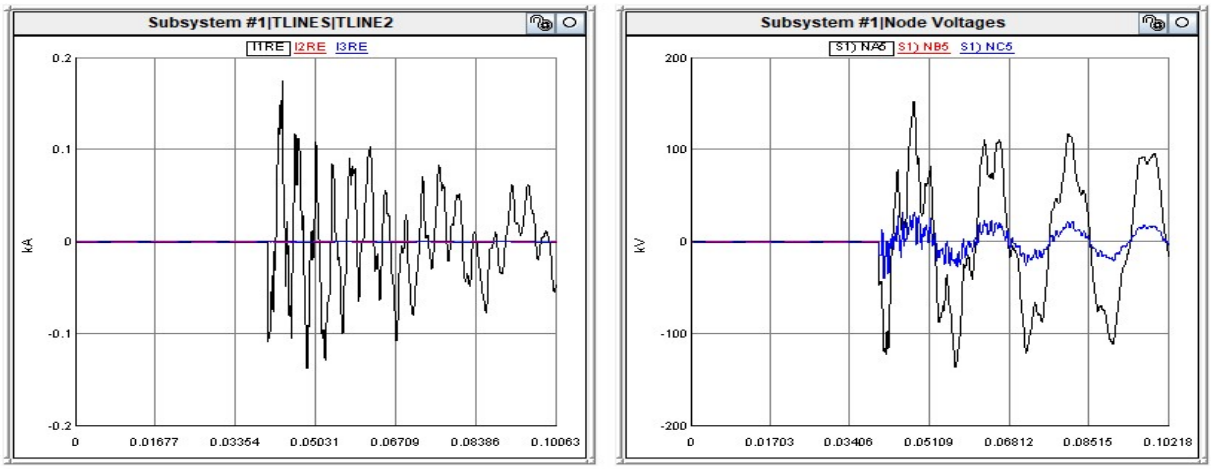

Figure 14:. Voltage and current waveforms at bus 5 after single phase OC fault

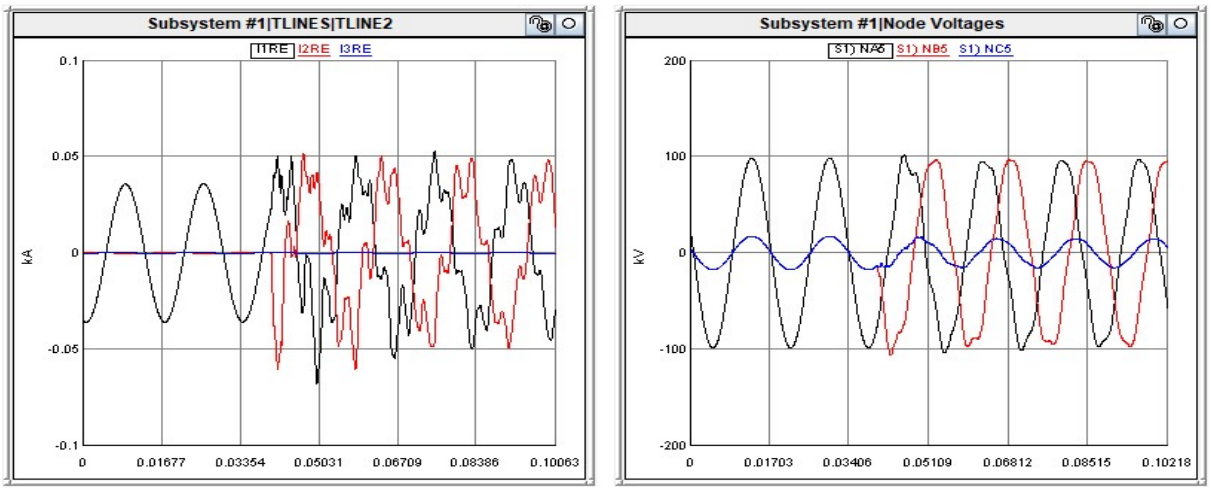

Fig. 15: Voltage and current waveform after two phase open conductor fault

The voltage and current waveforms in Figure14 and Figure 15 are for scenarios where a single-phase and two-phase open circuit fault have occurred, respectively. The power calculation for single conductor and two conductor open circuit fault are calculated as,

For single conductor OC fault

3-ϕ Complex Power $(S_{3-\varphi}) = V_a I_a + V_b I_b + V_c I_c$

3-ϕ Active Power = Real $(S_{3-\varphi})$ =3996.814 KW

3-ϕ Reactive Power = Img $(S_{3-\varphi}) = -36.54$Kvar

For two conductors OC fault

3-ϕ Complex Power $(S_{3-\varphi}) = V_a I_a + V_b I_b + V_c I_c$

3-ϕ Active Power = Real $(S_{3-\varphi})$ = 2226.814 KW

3-ϕ Reactive Power = Img $(S_{3-\varphi})$ = 26.48 Kvar

It is evident that in both single-conductor and two-conductor OC faults, the active power falls below the lower active power threshold, and similarly, the reactive power drops below the lower reactive power threshold. The proposed method is the most suitable method to protect power systems against failure of 1-conductor, 2-conductor or 3-conductor open-circuit and closed-circuit faults. Unlike impedance-based approaches, this method does not rely on knowing the grid's Thevenin's equivalent impedance. In addition, the proposed method is not affected by nonlinear dynamic behavior.

Another benefit of this method is its ability to accurately locate faults within an acceptable margin of error, identifying both open-circuit and closed-circuit issues. However, the effectiveness of the proposed method may be constrained by the precise positioning of PMUs within the power system and the optimal selection of PMU locations [41,42]. In addition, inaccuracies in measuring the voltage and current phasor can affect the estimation of faulty line impedance; thus, the proposed technique requires assessment. Moreover, the scheme does not provide information regarding the source or severity of the fault. To mitigate these limitations, the redundancy in the PMU network can be enhanced by installing additional PMUs at strategic points. This ensures that if one PMU fails, there is always a backup available to monitor the system [43,44]. Furthermore, the accuracy of PMUs can be enhanced through regular calibration and proper maintenance. To obtain information about the fault's source or severity, additional analysis could be conducted using multiple fault detection algorithms to determine appropriate corrective actions.

3.4. External Faults Beyond the Geographical Zone

The proposed techniques are also effective in identifying external faults occurring outside the designated geographical zone. By integrating the differential relay scheme, which is inherently capable of detecting external faults, the methodology ensures comprehensive fault monitoring. The detection process follows a similar approach as demonstrated in Figure16, 17, and 18. When an external fault such as LG, LL, or LLG occurs beyond the monitored zone, the signals recorded by PMUs within the zone remain nearly identical.

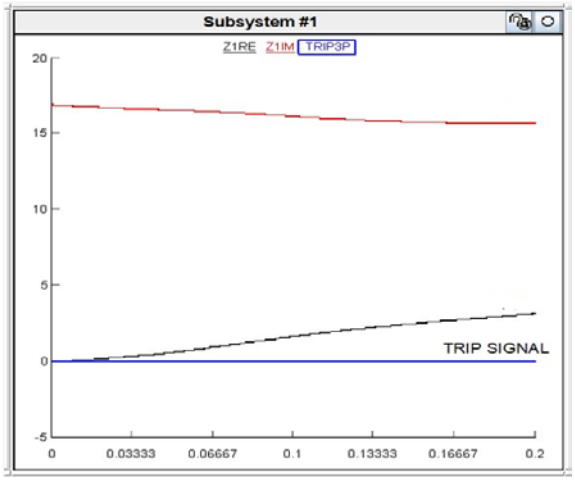

Fig. 16: Phasor value of Impedance for LG Fault occurred outside the zone

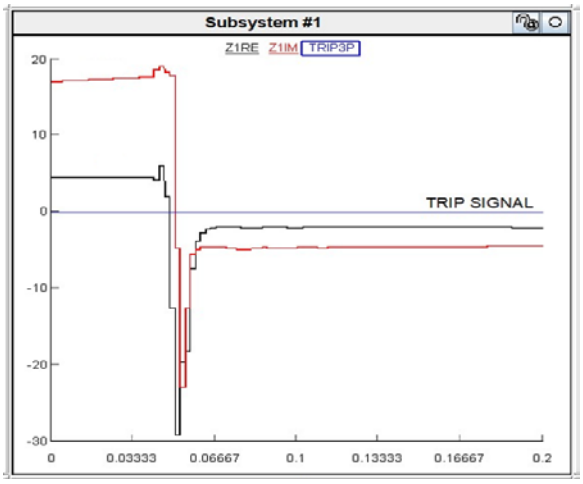

Fig. 17: Phasor value of Impedance for LL Fault occurred outside the zone

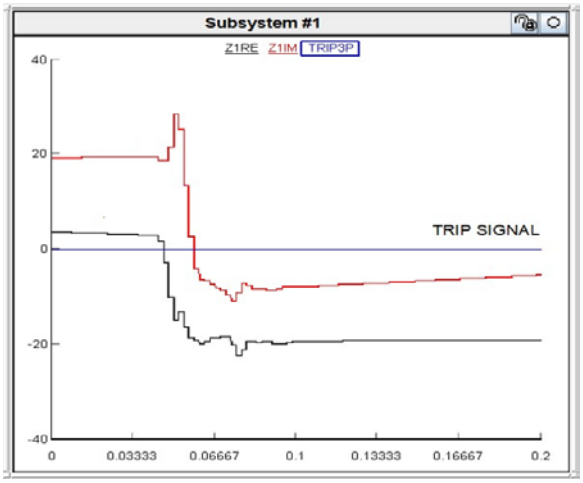

Fig. 18: Phasor value of Impedance for LLG Fault occurred outside the zone

As a result, the differential value calculated between the two buses inside the geographical zone remains zero, preventing the generation of a trip signal. This confirms that the fault is external, ensuring that unnecessary tripping within the protected zone is avoided

4. Conclusion

This research introduces an innovative fault detection and identification approach for power systems, leveraging Tellegen's theorem and PMUs. The proposed method divides the power system into zones and simultaneously analyzes each zone to rapidly and accurately detect faults. Tellegen's theorem is employed for fault identification calculations, utilizing faulty line impedance, while distance-to-fault calculations are utilized to precisely locate the fault site. The effectiveness of the proposed fault detection method was demonstrated by simulating the results obtained using the 8-bus test system. The purposed also affective to analyze the external fault that occurred outside the monitored zone. The algorithm successfully detected defects within acceptable margins and rapidly and accurately identified them. However, the proposed approach has some limitations, such as the cost associated with installing PMUs and the necessity for precise network models. The suggested fault detection and identification algorithm, which employs PMUs and Tellegen's theorem, has been demonstrated to be a promising method for overall power system fault detection. Future research might be extended validation IEEE-13 and IEEE-34 bus distribution systems. The proposed approach can also focus on enhancing the algorithm's precision and reliability, as well as investigating ways to reduce the cost of installing PMUs.

Acknowledgements

The author would like to extend my appreciation to Dr. Ikbal Ali for their inspiration and guidance throughout my research on the RTDS platform.

Nomenclature

PMU	Phasor Measurement Units
FI	Fault Identification
RTDS	Real-Time Digital Simulation
AI	Artificial Intelligence
OC	Open Circuit
P.T	Potential Transformer
PL	Active power lower threshold limit
ML	Machine Learning
QL	Reactive power lower threshold limit
BRK	Circuit Breaker
PH	Active power upper threshold limit
SC	Short Circuit
QH	Reactive power upper threshold limit
C.T	Current Transformer
Va, Vb, Vc	Three Phase voltage
Ia, Ib, Ic	Three phase current
Ia0, Ia1, Ia2	Zero, Positive, Negative sequence current
KW	Kilowatts

References

1) J.Li, and S. Jiang, “Global energy interconnection: an effective solution to climate challenges,” Global Energy Interconnection, 1 (4) 406–408 (2018). doi:10.1016/S2096-5117(18)30075-6.
2) I.ALI, M.A. AFTAB, and S.M.S. HUSSAIN, “Performance comparison of iec 61850-90-5 and ieee c37.118.2 based wide area pmu communication networks,” Journal of Modern Power Systems and Clean Energy, 4 (3) 487–495 (2016). doi:10.1007/s40565-016-0210-y.
3) R.Isermann, “Model-based fault-detection and diagnosis – status and applications,” Annu Rev Control, 29 (1) 71–85 (2005). doi:10.1016/j.arcontrol.2004.12.002.
4) S.Beheshtaein, R. Cuzner, M. Savaghebi, and J.M.

Guerrero, “Review on microgrids protection,” IET Generation, Transmission & Distribution, 13 (6) 743–759 (2019). doi:10.1049/iet-gtd.2018.5212.

5) B.J.Brearley, and R.R. Prabu, “A review on issues and approaches for microgrid protection,” Renewable and Sustainable Energy Reviews, 67 988–997 (2017). doi:10.1016/j.rser.2016.09.047.
6) L.Sun, and F. You, “Machine learning and data-driven techniques for the control of smart power generation systems: an uncertainty handling perspective,” Engineering, 7 (9) 1239–1247 (2021). doi:10.1016/j.eng.2021.04.020.
7) S.Kar, S.R. Samantaray, and M.D. Zadeh, “Data-mining model based intelligent differential microgrid protection scheme,” IEEE Syst J, 11 (2) 1161–1169 (2017). doi:10.1109/JSYST.2014.2380432.
8) M.Mansouri, M.-F. Harkat, H.N. Nounou, and M.N. Nounou, “Model-based approaches for fault detection,” in: Data-Driven and Model-Based Methods for Fault Detection and Diagnosis, Elsevier, 2020: pp. 221–258. doi:10.1016/B978-0-12-819164-4.00015-7.
9) M.Hojabri, U. Dersch, A. Papaemmanouil, and P. Bosshart, “A comprehensive survey on phasor measurement unit applications in distribution systems,” Energies (Basel), 12 (23) 4552 (2019). doi:10.3390/en12234552.
10) S.Samantaray, and N.K. Sharma, “PMU Assisted Integrated Impedance Angle-Based Microgrid Protection Scheme,” in: 2022 IEEE Power & Energy Society General Meeting (PESGM), IEEE, 2022: pp. 1–1. doi:10.1109/PESGM48719.2022.9916954.
11) Y.Bansal, and R. Sodhi, “PMUs enabled tellegen’s theorem-based fault identification method for unbalanced active distribution network using rtds,” IEEE Syst J, 14 (3) 4567–4578 (2020). doi:10.1109/JSYST.2020.2976736.
12) H.F.Habib, M.M. Esfahani, and O. Mohammed, “Development of Protection Scheme for Active Distribution Systems with Penetration of Distributed Generation,” in: SoutheastCon 2018, IEEE, 2018: pp. 1–7. doi:10.1109/SECON.2018.8479115.
13) A.Soleimanisardoo, H. Kazemi Karegar, and H.H. Zeineldin, “Differential frequency protection scheme based on off-nominal frequency injections for inverter-based islanded microgrids,” IEEE Trans Smart Grid, 10 (2) 2107–2114 (2019). doi:10.1109/TSG.2017.2788851.
14) S.Kumar, I. Ali, and A. Siddiqui, “Protection of microgrid feeders using impedance angle analysis assisted by synchrophasor units,” Journal of Renewable Energy and Environment, 11 (3) 109–119 (2024). doi:10.30501/jree.2024.432832.1794.
15) C.Wang, M. Wang, B. Yang, and K. Song, “A model-based method for bearing fault detection using motor current,” J Phys Conf Ser, 1650 (3) 032130 (2020). doi:10.1088/1742-6596/1650/3/032130.
16) X.G.Magagula, Y. Hamam, J.A. Jordaan, and A.A. Yusuff, “Fault detection and classification method using DWT and SVM in a power distribution network,” in: 2017 IEEE PES PowerAfrica, IEEE, 2017: pp. 1–6. doi:10.1109/PowerAfrica.2017.7991190.
17) T.Nagpal, and Y.S. Brar, “Expert system based fault detection of power transformer,” J Comput Theor Nanosci, 12 (2) 208–214 (2015). doi:10.1166/jctn.2015.3719.
18) X.Fan, and M.J. Zuo, “Fault diagnosis of machines based on d–s evidence theory. part 1: d–s evidence theory and its improvement,” Pattern Recognit Lett, 27 (5) 366–376 (2006). doi:10.1016/j.patrec.2005.08.025.
19) M.R.Zaidan, “Power System Fault Detection, Classification And Clearance By Artificial Neural Network Controller,” in: 2019 Global Conference for Advancement in Technology (GCAT), IEEE, 2019: pp. 1–5. doi:10.1109/GCAT47503.2019.8978400.
20) X.Wang, Z. Li, J. Liang, and Y. Li, “A Deep Double-Convolutional Neural Network-Based Fault Detection,” in: 2023 IEEE 2nd Industrial Electronics Society Annual On-Line Conference (ONCON), IEEE, 2023: pp. 1–6. doi:10.1109/ONCON60463.2023.10431392.
21) N.Ramesh Babu, and B. Jagan Mohan, “Fault classification in power systems using emd and svm,” Ain Shams Engineering Journal, 8 (2) 103–111 (2017). doi:10.1016/j.asej.2015.08.005.
22) H.A.Illias, X.R. Chai, and A.H. Abu Bakar, “Hybrid modified evolutionary particle swarm optimisation-time varying acceleration coefficient-artificial neural network for power transformer fault diagnosis,” Measurement, 90 94–102 (2016). doi:10.1016/j.measurement.2016.04.052.
23) M.Korkali, H. Lev-Ari, and A. Abur, “Traveling-wave-based fault-location technique for transmission grids via wide-area synchronized voltage measurements,” IEEE Transactions on Power Systems, 27 (2) 1003–1011 (2012). doi:10.1109/TPWRS.2011.2176351.
24) S.Saha, A. Bag, D. Basu Roy, S. Patranabis, and D. Mukhopadhyay, “Fault Template Attacks on Block Ciphers Exploiting Fault Propagation,” in: 2020: pp. 612–643. doi:10.1007/978-3-030-45721-1_22.
25) G.Chen, Q. Duan, C. Zhao, H. Wang, G. Sha, J. Gao, Y. Li, and S. Zhou, “Novel fault protection method for flexible dc power systems,” Energies (Basel), 17 (14) 3446 (2024). doi:10.3390/en17143446.
26) S.Pan, T. Morris, and U. Adhikari, “Classification of disturbances and cyber-attacks in power systems using heterogeneous time-synchronized data,” IEEE

Trans Industr Inform, 11 (3) 650–662 (2015). doi:10.1109/TII.2015.2420951.

27) T.Yildiz, and A. Abur, “Convolutional neural network-assisted fault detection and location using few pmus,” Electric Power Systems Research, 235 110705 (2024). doi:10.1016/j.epsr.2024.110705.
28) I.Pavičić, N. Holjevac, I. Ivanković, and D. Brnobić, “Model for 400 kv transmission line power loss assessment using the pmu measurements,” Energies (Basel), 14 (17) 5562 (2021). doi:10.3390/en14175562.
29) Y.Shu, and W. Chen, “Research and application of uhv power transmission in china,” High Voltage, 3 (1) 1–13 (2018). doi:10.1049/hve.2018.0003.
30) M.B.K.Bouzid, and G. Champenois, “New expressions of symmetrical components of the induction motor under stator faults,” IEEE Transactions on Industrial Electronics, 60 (9) 4093–4102 (2013). doi:10.1109/TIE.2012.2235392.
31) M.Majidi, and M. Etezadi-Amoli, “A new fault location technique in smart distribution networks using synchronized/nonsynchronized measurements,” IEEE Transactions on Power Delivery, 33 (3) 1358–1368 (2018). doi:10.1109/TPWRD.2017.2787131.
32) M.Memarzadeh, B. Matthews, and I. Avrekh, “Unsupervised anomaly detection in flight data using convolutional variational auto-encoder,” Aerospace, 7 (8) 115 (2020). doi:10.3390/aerospace7080115.
33) J.-D.Park, and J. Candelaria, “Fault detection and isolation in low-voltage dc-bus microgrid system,” IEEE Transactions on Power Delivery, 28 (2) 779–787 (2013). doi:10.1109/TPWRD.2013.2243478.
34) Z.Huang, and Z. Wang, “A multiswitch open-circuit fault diagnosis of microgrid inverter based on slidable triangularization processing,” IEEE Trans Power Electron, 36 (1) 922–930 (2021). doi:10.1109/TPEL.2020.3004531.
35) S.A.Hosseini, H.A. Abyaneh, S.H.H. Sadeghi, F. Razavi, and A. Nasiri, “An overview of microgrid protection methods and the factors involved,” Renewable and Sustainable Energy Reviews, 64 174–186 (2016). doi:10.1016/j.rser.2016.05.089.
36) N.Sonule, and Prof.V. Madekar, “Short circuit fault detection and protection of dc microgrid,” Int J Res Appl Sci Eng Technol, 11 (6) 4082–4087 (2023). doi:10.22214/ijraset.2023.54397.
37) S.Das, S. Santoso, A. Gaikwad, and M. Patel, “Impedance-based fault location in transmission networks: theory and application,” IEEE Access, 2 537–557 (2014). doi:10.1109/ACCESS.2014.2323353.
38) S.H.Mortazavi, and J. Sadeh, “An analytical fault location method based on minimum number of installed pmus,” International Transactions on Electrical Energy Systems, 26 (2) 253–273 (2016). doi:10.1002/etep.2075.
39) S.Das, S.P. Singh, and B.K. Panigrahi, “Transmission line fault detection and location using wide area measurements,” Electric Power Systems Research, 151 96–105 (2017). doi:10.1016/j.epsr.2017.05.025.
40) Y.Bansal, and R. Sodhi, “PMUs enabled tellegen’s theorem-based fault identification method for unbalanced active distribution network using rtds,” IEEE Syst J, 14 (3) 4567–4578 (2020). doi:10.1109/JSYST.2020.2976736.
41) W.Li, D. Deka, M. Chertkov, and M. Wang, “Real-time faulted line localization and pmu placement in power systems through convolutional neural networks,” IEEE Transactions on Power Systems, 34 (6) 4640–4651 (2019). doi:10.1109/TPWRS.2019.2917794.
42) C.Allioua, A. Mingotti, R. Tinarelli, L. Peretto, and G. Frigo, “Cloud-Based PMUs for Real-Time Power System Monitoring: Theoretical and Experimental Analysis,” in: 2023 IEEE 13th International Workshop on Applied Measurements for Power Systems (AMPS), IEEE, 2023: pp. 01–06. doi:10.1109/AMPS59207.2023.10297270.
43) S.Ghosh, Y.J. Isbeih, S.K. Azman, M.S. El Moursi, and E. El-Saadany, “Optimal pmu allocation strategy for completely observable networks with enhanced transient stability characteristics,” IEEE Transactions on Power Delivery, 37 (5) 4086–4102 (2022). doi:10.1109/TPWRD.2022.3144462.
44) E.Casagrande, W.L. Woon, H.H. Zeineldin, and D. Svetinovic, “A differential sequence component protection scheme for microgrids with inverter-based distributed generators,” IEEE Trans Smart Grid, 5 (1) 29–37 (2014). doi:10.1109/TSG.2013.2251017.